

Reinforced Imitation: Sample Efficient Deep Reinforcement Learning for Map-less Navigation by Leveraging Prior Demonstrations

M. Pfeiffer^{1*}, S. Shukla^{2*}, M. Turchetta³, C. Cadena¹, A. Krause³, R. Siegwart¹, J. Nieto¹

Abstract—This work presents a learning-based approach for target driven map-less navigation. The underlying navigation model is an end-to-end neural network which is trained using a combination of expert demonstrations, imitation learning (IL) and reinforcement learning (RL). While RL and IL suffer from a large sample complexity and the distribution mismatch problem, respectively, we show that pre-training the navigation model using expert demonstrations can reduce the training time to reach at least the same level of performance compared to plain RL by a factor of 5. We present a thorough evaluation of different combinations of expert demonstrations and RL, both in simulation and on a real robotic platform. Our results show that the final model outperforms both standalone approaches in the amount of successful navigation tasks. The learned navigation policy is also able to generalize to unseen and real-world environments.

I. INTRODUCTION

Autonomous navigation in environments where global knowledge of the map is available is nowadays well understood [1]. Optimization objectives like, e.g., minimum path length, travel time or safe distance to obstacles can be used to find the optimal path connecting the start and goal position of a robot. However, full knowledge of the map is not always available in practice. Given only local perception around the robot and a relative target position, robust map-less navigation strategies are required. In recent years, machine learning techniques — with neural networks leading the way [2]–[4] — have gained importance allowing for the application of end-to-end motion planning approaches. Instead of splitting the navigation task into multiple sub-modules like, e.g., sensor fusion, obstacle detection, global and local motion planning, end-to-end approaches use a direct mapping from sensor data to robot motion commands which can reduce the complexity during deployment significantly.

Current state-of-the-art end-to-end planning approaches can be split in two major groups: (i) imitation learning (IL) based ones use supervised learning techniques to imitate expert demonstrations as close as possible, and (ii) approaches based on reinforcement learning (RL) where the agents learn their navigation policy by trial and error exploration combined with reward signals. IL is sample efficient and can achieve accurate

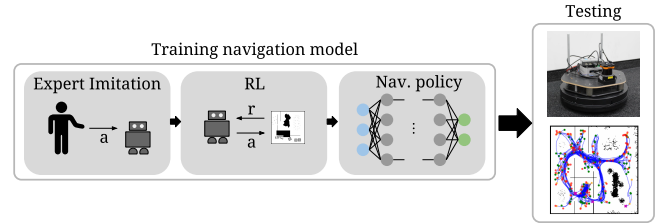


Fig. 1: An end-to-end navigation policy is learned from a combination of imitation and reinforcement learning. The resulting policy is tested thoroughly in simulation and on a real robotic platform.

imitation of the expert demonstrations. Given the training data, satisfactory navigation models can be found within a few hours of training [2]. However, it is likely to overfit to the environment and situations presented at training time. This limits the potential for generalization and the robustness of the policy (distribution mismatch). RL is more robust — also in unseen scenarios — as the agent learns from its own mistakes during training [3]. The disadvantage of RL is its sample inefficiency, limiting the current utilization to applications where training can be conducted using extremely fast simulators [5].

In this work, we present an approach that combines the advantages of both IL and RL. It is inspired by human learning, which typically combines the observation of other people and self-exploration [6].

Our approach, in the following called *reinforced imitation learning (R-IL)*, combines supervised IL based on expert demonstrations to pre-train the navigation policy with subsequent RL. For RL, we use Constrained Policy Optimization (CPO) [7] due to its ability to incorporate constraints during training, which is especially important to avoid collisions during navigation.

We hypothesize that the combination of the two learning approaches yields a more robust policy than pure IL, and that it is also easier and faster to train than pure RL. To the best of our knowledge, this is the first work to explore this combination for robot navigation. We provide an extensive evaluation of the training and navigation performance in simulation and on a robotic platform. Our main contributions are:

- a learning framework combining IL and RL¹
- a model for map-less end-to-end motion planning that generalizes to unseen environments
- an extensive evaluation of training and generalization performance to unseen environments

This paper is structured as follows: In Section II, we present

¹Our source code will be made available to the public together with the final release of this paper.

This work has received funding from the European Union Horizon 2020 project CROWDBOT, Grant No. 779942.

*The authors contributed equally to this work.

¹The authors are with the Autonomous Systems Lab, ETH Zurich, Zurich, Switzerland.

²The author is with the Computer Vision Lab, ETH Zurich, Zurich, Switzerland.

³The authors are with the Learning & Adaptive Systems Group, ETH Zurich, Zurich, Switzerland.

{pfeiffer, shuklas, matteotu, cesarc, krausea, rsiegwart, nietoj}@ethz.ch.

the related work. Section III presents the problem and our proposed approach. In Section IV we show our experiments and evaluations before the conclusions are drawn in Section V.

II. RELATED WORK

In this section we give an overview of the existing work in the areas of learning by demonstration and RL in connection to the navigation problem with a focus on end-to-end techniques. Furthermore, we present the most related approaches combining IL and RL for other applications.

A. Learning by demonstration

Learning by demonstration can be split in two main areas: (i) inverse reinforcement learning (IRL), where a reward function is inferred from expert demonstrations and a policy is derived by optimizing this reward with optimal control techniques and (ii) IL, where expert demonstrations are used to directly infer a policy. Abbeel *et al.* [8] present an IRL-based approach where they teach an autonomous car to navigate in parking lots by observing human demonstrations. Similarly, Pfeiffer *et al.* [9] and Kretzschmar *et al.* [10] present approaches for navigation in dynamic environments based on IRL. By observing pedestrian motion, a probability distribution over pedestrian trajectories is found. For path planning, the trajectory with the highest probability according to the learned model is chosen with the goal of a close imitation of pedestrian motion. Wulfmeier *et al.* [11] present a similar approach using deep IRL instead of a combination of classical features in order to learn how to drive an autonomous car through static environments.

In the following, we give an overview of the literature on map-less navigation using IL. Muller *et al.* [4] present an image-based approach for end-to-end collision avoidance using imitation learning. In their work, the focus is on feature extraction and on generalization to new situations. The overall navigation performance of such approaches is not analyzed. Another approach focused on perception is presented by Chen *et al.* [12]. They combine learning-based feature extraction using convolutional neural networks (CNNs) with a classical driving controller for an autonomous car. However, they focus on a lane-following application and do not deal with target-driven navigation. Kim *et al.* [13] present an IL approach for hallway navigation and collision avoidance for an unmanned aerial vehicle (UAV). They show a working model on a real-world platform, yet the environmental setup is relatively easy and no real navigation capabilities are required. Similarly, Sergeant *et al.* [14] present an end-to-end approach for laser-based collision avoidance for ground vehicles. The collision avoidance capabilities of the learned models are shown both in simulation and real-world tests. However, they do not take into account any target information and therefore the approach cannot be used for target-driven navigation. Ross *et al.* [15] present the Dataset Aggregation (DAGGER) method which collects demonstrations according to the currently best policy but can also query additional expert demonstrations in order to alleviate the distribution mismatch problem. This approach can also be extended to online learning. One application of the DAGGER algorithm

is presented in [16], where directional commands for forest navigation and collision avoidance are learned from expert demonstrations.

The method we introduce builds upon prior work presented in [2], where a global planner is used to generate expert demonstrations in simulation. Given demonstrations, an end-to-end navigation policy mapping from 2D laser measurements and a relative goal position to motion commands is found. The main drawbacks of this approach are the generalization to new environments — also due to the specific CNN model structure — and the behavior in situations which were not covered in the training data (distribution mismatch).

B. Reinforcement learning

Bischoff *et al.* [17] use ideas from hierarchical RL to decompose the navigation task in motion planning and movement execution and thus are able to improve the sample efficiency of plain RL. Yet global map information is always assumed to be known. Zuo *et al.* [18] use a popular model-free RL algorithm, Q-learning, to teach a robot a policy to navigate through a simple spiral maze from sonar inputs only.

Mirowski *et al.* [19] use auxiliary tasks such as depth prediction and loop closure assessment to improve the learning rate of A3C [5] for simulated maze navigation from RGB images. Bruce *et al.* [20] use interactive experience replay to learn how to navigate in a known environment to a fixed goal from images by traversing it only once. The method presented in [21] focuses on efficient knowledge transfer across maps and conditions for an autonomous navigation task. To this end, it uses a particular parametrization of the Q-function, known as successor representation, that decouples task specific knowledge from transferable knowledge. Zhu *et al.* [22] present an end-to-end vision-based navigation algorithm that uses the target as an additional input to the policy to learn to achieve proper target-driven navigation.

The method presented by Tai *et al.* [3] is the most closely related to ours. In our work, the Asynchronous Deep Deterministic Policy Gradients algorithm is used to learn a policy from range findings to continuous steering commands for both simulated and real-world map-less navigation tasks.

As experiments in robotics usually require large amounts of time, the problem of reducing the sample complexity of RL based approaches has received increasing attention recently. Using a combination of IL and RL to obtain a sample efficient and robust learning algorithm has previously been explored in robotics in the context of manipulation tasks [23], [24]. To the best of our knowledge, our method is the first to use expert demonstrations to boost RL learning performance in the context of map-less autonomous navigation.

III. APPROACH

A. Problem formulation

Classical path planning techniques [1] require prior knowledge of the environment for navigation. In case of constantly changing environments, maintaining an accurate map representation becomes increasingly difficult or even unfeasible. In such situations, map-less navigation skills based solely on

local information available to the robot through its sensors are required.

The underlying problem is the following: Given the sensor measurements \mathbf{y} and a relative target position \mathbf{g} , we want to find a policy π_{θ} parametrized by θ which maps these inputs to suitable control commands, \mathbf{u} , i.e. a function

$$\mathbf{u} = \pi_{\theta}(\mathbf{y}, \mathbf{g}). \quad (1)$$

The required control commands are comprised of the translational and rotational velocity.

As the mapping from local sensor and target data to control commands can be arbitrarily complex, learning how to plan from experience in an end-to-end fashion using powerful non-linear function approximators, such as neural networks, has become more prominent within the last decade. In this work, we aim at combining IL and RL to obtain a sample efficient and robust learning based navigation algorithm. We do this in a sequential fashion by using the result from IL to initialize our RL method. In the remainder of this section we introduce separately the underlying neural network model, the IL and RL components of our method.

B. Neural network model

The neural network model which is used to map sensor measurements and target information to control commands, is shown in Figure 2. In this work, the inputs to the model are 2D laser range findings and a relative target position in polar coordinates w.r.t. the local robot coordinate frame. In contrast to [2], where a CNN was used to extract environmental features, this model is simplified and only relies on three fully connected layers. While the CNN allows to find relevant environmental features, we found that it tends to overfit to the shapes of the obstacles presented during training. Instead, we use minimum pooling of the laser data and compress the full range of 1080 measurements into 36 values, where each pooled value $\mathbf{y}_{p,i}$ is computed as:

$$\mathbf{y}_{p,i} = \min(\mathbf{y}_{i \cdot k}, \dots, \mathbf{y}_{(i+1) \cdot k}), \quad (2)$$

where i is the value index and k is the kernel size for 1D pooling. In our case, we chose $k = 30$. By taking the minimum of each angular interval, safety can still be assured. Nevertheless, detailed environmental features may get lost. The resulting simplified neural network model can be trained more efficiently and is less likely to overfit to specific obstacle shapes, which was one problem found in [2].

Furthermore, the inputs are normalized before being fed to the neural network model. The pooled laser measurements are cropped and then mapped to lie in the interval $[-1, 1]$. The relative target position is normalized in order to lie in the same interval. To map the output of the neural network, which also lies in the interval $[-1, 1]$, to translational and rotational velocities, we add a de-normalization step. For IL training, we also introduce a 50% dropout.

C. Supervised pre-training by imitation learning

In order to improve the performance and sample complexity of the succeeding RL, the neural network model is pre-trained using supervised IL based on expert demonstrations, similar

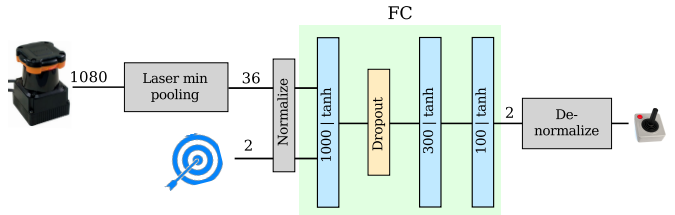


Fig. 2: The neural network model used to represent π_{θ} . The normalized input data is fed through three fully connected layers of different dimensions and with tanh activation functions. Between layer one and two, dropout is added during IL training. In order to obtain physical control commands from the neural network, the outputs need to be de-normalized.

to [2]. The loss function for supervised training is given by the sum of absolute error values of translational and rotational velocities, namely

$$L(\theta) = \mathbf{1}^T \cdot |\pi_{\theta}(\mathbf{y}, \mathbf{g}) - \mathbf{u}_{\text{exp}}|, \quad (3)$$

where \mathbf{u}_{exp} is the control applied by the expert when it receives (\mathbf{y}, \mathbf{g}) as input. This loss is the difference between the predicted and the expert motion commands given the observation and target inputs. The goal is to imitate the expert as closely as possible, given the representation limitations of the neural network model. Yet, using plain IL, the performance of the final model will always be limited by the performance of the expert demonstrations. The advantage of R-IL over IL is that this limitation can be overcome through self-improvement. The output of this IL policy is deterministic and no further sampling actions are conducted.

D. Reinforcement learning

1) *Background information:* Given a Markov Decision Process (MDP), $M = \langle \mathcal{S}, \mathcal{A}, \mathcal{P}, \mathcal{R}, \gamma \rangle$, where \mathcal{S} is the state space, \mathcal{A} is the action space, $\mathcal{P}(\cdot | s_t, a_t) : \mathcal{S} \times \mathcal{S} \times \mathcal{A} \rightarrow \mathbb{R}_+$ is the transition probability distribution, $\mathcal{R}(\cdot, \cdot) : \mathcal{S} \times \mathcal{A} \rightarrow \mathbb{R}$ is the reward function for a given state action pair and $\gamma \in [0, 1]$ is the discount factor, the goal of RL is to find a policy π_{θ} , which maps observations to actions, that maximizes the expected sum of discounted rewards, given by

$$J(\theta) = \mathbb{E} \left[\sum_{t=0}^T \gamma^t \cdot r(s_t, \pi_{\theta}(s_t)) \right], \quad (4)$$

where T is the time horizon of a navigation episode. In our case, s_t is defined by the sensor measurements and the target information, a_t by the control commands.

Policy gradient methods [25] are a popular set of model-free RL algorithms. They use the empirical estimate of the gradient of $J(\theta)$ with respect to the policy parameters θ to update the policy at each iteration using modifications of stochastic gradient descent.

However, classical policy gradient methods [25] suffer from a high variance in gradients, resulting in undesirably large updates to the policy which may lead to poor performance. A popular technique to reduce model variance and ensure stability between updates is Trust Region Policy Optimization (TRPO) [26]. It restricts the change in policy at each update by imposing a constraint on the average Kullback-Leibler (KL) divergence between the new policy and old policy, which results in more stable policy updates.

Enforcing safety is highly prioritized and strictly necessary when dealing with robotics applications. Therefore, we want to be able to incorporate constraints in our learning algorithm. Given a cost function $C : \mathcal{S} \times \mathcal{A} \rightarrow \mathbb{R}$, let $J_C(\theta)$ indicate the expected discounted return of the policy with respect to this cost

$$J_C(\theta) = \mathbb{E} \left[\sum_{t=0}^T \gamma^t \cdot C(s_t, \pi_\theta(s_t)) \right]. \quad (5)$$

In constrained MDPs we aim at finding

$$\theta^* = \arg \max J(\theta), \quad s.t. \quad J_C(\theta) \leq \alpha. \quad (6)$$

Constrained Policy Optimization (CPO) [7] is a RL algorithm that finds an approximate solution to the problem in Eq. 6 by extending ideas from TRPO to constrained MDPs.

2) *Training process*: For training, the neural network model is first initialized either randomly (pure RL) or using IL (R-IL). A stochastic policy is used where the actions are sampled from a 2D Gaussian distribution having the de-normalized values of the output of the neural network as mean, and a 2D standard deviation which is a separate learn-able parameter. Using a supervised IL model thus only influences the initialization of the RL policy. During training we randomly select a start and target position and collect robot experience samples by running an episode using the current policy π_θ for a fixed number of time steps or until the robot reaches the target. At each iteration of the policy update, a batch consisting of samples collected from multiple episodes is used.

The agent’s objective is to learn to reach the target in the shortest possible number of time-steps while avoiding collisions with surrounding obstacles. The reward function provides the required feedback to the robot during the learning process. The desired behavior to successfully reach the target is encouraged by giving a positive reward when the robot reaches the target. However, having a sparse reward for final success makes the learning process difficult as the agent struggles to differentiate which actions had a positive or negative effect toward the accomplishment of the task. Therefore, the reward function is shaped to provide continuous feedback for each action by rewarding/penalizing the agent for getting closer/further to/from the goal from the current location along the shortest feasible path. Let $d(s)$ denote the distance from s to the goal along the shortest feasible path to the target, which takes into account the position of obstacles in the map and is computed using the Dijkstra algorithm [27]. The combined reward function is given by:

$$r(s_t) = \begin{cases} 10, & \text{if success} \\ -(d(s_t) - d(s_{t-1})), & \text{otherwise} \end{cases}$$

Note, the agent does not have any knowledge about $d(\cdot)$. This distance is only used to compute the reward which the agent receives from the environment during training.

In order to learn collision avoidance, using a negative reward for collisions makes the learned behavior highly sensitive to this reward’s magnitude, resulting in a delicate trade-off between two different objectives — reaching the target and avoiding crashes. However, in constrained MDPs, we

can encode collision avoidance through a constraint on the expected number of crashes allowed per episode. Let $\mathcal{S}_c \subset \mathcal{S}$ denote the set of states that correspond to a crash. We define a state depended cost function as follows:

$$c(s_t) = \mathcal{I}(s_t \in \mathcal{S}_c), \quad (7)$$

where \mathcal{I} is the indicator function. By setting the discount factor for the cost — which does not have to be equal to the one for the reward — to 1 and introducing the constraint value α , we can constrain the number of expected crashes per episode to be less or equal to α . In our model we set $\alpha = 0.4$. While training, we allow for multiple crashes in each episode. This leads to more crash samples in the training set which allows the robot to learn collision avoidance behavior at a faster rate, thus making the training process more efficient.

E. Training in simulation

The models are purely trained in simulation since there are no space constraints, the environment structure can be changed arbitrarily, and it is a faster and more efficient way of training and evaluating the model. The agent learns collision avoidance through its own experiences. Since during the training phase, the robot will crash repeatedly with surrounding obstacles, doing so in a real environment may damage the robot and the environment. Moreover, the trained model may not have the desired behavior, due to mis-specification of the reward function or data inefficiency [28]. Models trained in simulation have previously been shown to successfully transfer to the real-world [2], [3], [29].

IV. EXPERIMENTS

This section presents the experiments conducted in simulation and on the real robotic platform. In these experiments, various models based on different training procedures are analyzed. The goal of the experiments is to investigate the influence of pre-training the RL models using IL and verify whether the training time can be reduced or the performance can be increased. Furthermore, we investigate the generalization performance of the navigation policies to unseen scenarios and also the transfer from experiments in simulation to the real world, which is also shown in our video². Our work does not intend to show that we can outperform a global graph-based planner in known environments, where graph-based solutions are fast and can achieve optimal behavior. The goal of our experiments is to investigate the limits of motion planning with local information only.

A. Experimental setup

All the models are trained solely in simulation and either tested in simulation or on a robotic platform. The experiments are based on a differential drive Kobuki TurtleBot2³ platform equipped with a front-facing Hokuyo UTM laser range finder with a field of view of 270°, maximum scanning range of 30m and 1080 range measurements per revolution. For on-board computations we resort to an Intel® NUC with an i7-5557U processor and without any GPU, running Ubuntu 14.04

²<https://youtu.be/uc386uZCgEU>

³<http://kobuki.yujinrobot.com/about2>

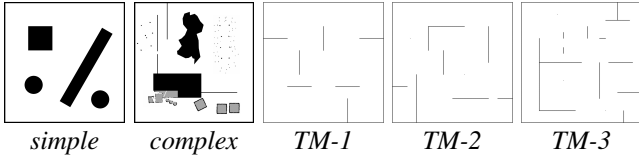


Fig. 3: Training maps for IL and RL. Although the *TM* maps appear similar, they vary significantly in difficulty. Maps can be better viewed by zooming in on a computer screen.

and ROS [30] as a middleware. The motion commands are published with a frequency of 5 Hz.

B. Model training

As mentioned above, different procedures for model training are applied: (i) pure IL, (ii) pure RL and (iii) R-IL, which is a combination of both. In order to test the influence of the complexity and the diversity of the training environments on test performance, we train the models on five maps (or subsets of them) as shown in Figure 3. The pure IL models are trained in the *simple* and *complex* maps, the RL part happens in all three *TM* maps. Similarly, for R-IL, the IL part happens in the *simple* and *complex* maps and the RL part takes place in the *TM* maps. The reason for this separation is to investigate whether general navigation capabilities can be learned during the IL phase and transferred between maps during training or whether the IL initialization only helps if the expert demonstrations originate from the same map as used in RL.

The expert demonstrations used for IL are generated using the ROS `move_base`⁴ navigation stack to navigate between random start and target positions, as presented in [2]. We decided to use an expert planner instead of a human to make the demonstrations more consistent and time efficient. Table I summarizes all the models we trained. For each model, it indicates how many expert trajectories (if any) were provided and on which maps they were generated. Moreover, it specifies, for each model, the number of iterations (if any) CPO was run for and on which maps. As Table I suggests, the expert demonstrations range from only 10 trajectories on the *simple* map up to 1000 trajectories on the *complex* map. This variation allows us to estimate the influence of the amount and complexity of prior demonstrations. Given the demonstrations, one training iteration during IL takes around 7 ms on a computer equipped with an Intel® i7-7700K processor and a Nvidia GeForce GTX 1070 GPU. Therefore, training a policy via IL using 1000 expert trajectories took slightly more than 2.5 hours as 1.5 M iterations were used. For the model $s_{10}+RL$, only 500 training iterations were used, resulting in a training time of only one hour. The recording time of the expert demonstrations has to be added to end up with the overall time required.

During the RL part, the model training is performed on the *TM* maps (see Figure 3). For each training episode, the map is uniformly sampled from the three candidates (except for RL1) in order to provide a combination of easy and difficult navigation examples and more expressive reward information. One training iteration takes around 180s using the accelerated

TABLE I: Training details of the models, including the maps and number of trajectories used for IL and the maps and number of iterations used for RL.

	model code	IL-map(s)	#IL traj.	RL map(s)	# RL iter.
R-IL	$s_{10}+RL$	simple	10	1+2+3	1000
	$s_{1000}+RL$	simple	1000	1+2+3	1000
	$c_{1000}+RL$	complex	1000	1+2+3	1000
	$123_{1500}+RL$	1+2+3	500 each	1+2+3	1000
	$s_{10}+RL$	simple	10	1+2+3	200
	$c_{1000}+RL$	complex	1000	1+2+3	200
IL	s_{10}	simple	10	—	0
	c_{1000}	complex	1000	—	0
RL	RL1	—	0	1	1000
	RL123	—	0	1+2+3	1000

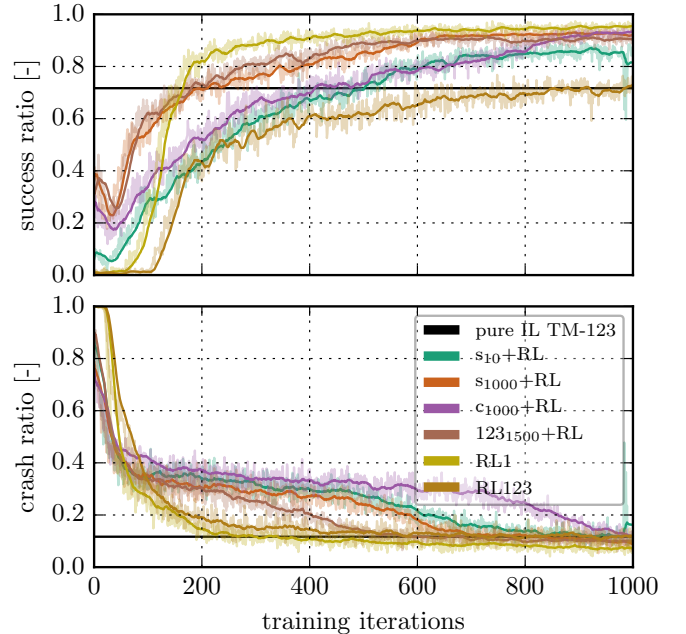


Fig. 4: The evolution of navigation success and crash rates throughout the RL training process of various models. The models contain two pure RL models, where one was trained in a simple environment and the other one in a combination of three environments. The R-IL models differ in the amount and complexity of expert demonstrations used for pre-training the model before RL. The black line indicates the performance of IL on the training maps (*TM-123*) as a reference.

Stage [31] simulation. During each iteration, we consider a batch consisting of 60 000 time steps. Therefore, 1000 iterations require around 50 hours of training time using the simulation, which is a real-time equivalent of around 100 days. This further motivates the need to find a good model initialization by IL in order to bring down the training time significantly.

Figure 4 shows the success and crash rates of the different models during RL training alongside the performance of pure IL trained on all *TM* maps. This pure IL model is not included in Table I and is not tested in the testing environment. Its only purpose is to serve as a baseline to evaluate the progress of the RL and IRL methods during training. Figure 4 clearly shows the difference between the models which were pre-trained using IL and the ones based on pure RL using CPO. While the pre-trained models already start at a certain success rate (depending on the performance of the IL model), it takes a significant amount of iterations for the RL models to reach the target in the majority of the cases. It may seem counter-intuitive that the RL1 model ends up outperforming all the

⁴http://wiki.ros.org/move_base

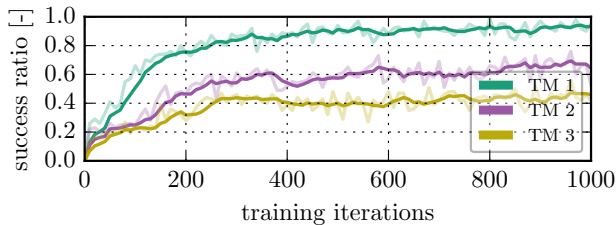


Fig. 5: Individual evaluation on the training maps based on the $c_{1000}+RL$ model. Success of the intermediate models are compared every 10 training iterations on each of the training maps. The difference in success rates clearly indicates the change in complexity between the three training maps.

others. This is due to the fact that this is the only model that is trained exclusively on the simplest map ($TM1$) in the TM map sets. As a consequence, it can be expected to perform very well during the training phase. However, it will be shown shortly that this model does not generalize well to more complex test environments. On the other hand, RL_{123} , which is trained on all three TM maps, does not reach the same convergence rate nor final performance during training.

One common characteristic of all R-IL models is a drop in the success rate after around 20-50 iterations before a significant increase of the success rate happens. Initially, the cost that defines the safety constraint 7 used in CPO has very high values and the agent learns to satisfy it. Therefore, in this phase, the agent learns to avoid crashes and unlearns the behavior of reaching the target, which is also supported by the crash rate curves in Figure 4. Once the policy reaches a performance where the collision constraint is fulfilled better, it again starts to learn to reach the target.

Interestingly, RL_{123} reaches approximately the same level of success and crash rates as a model which is trained using IL on the same maps. However, while all models converge to approximately the same crash rate, the R-IL models show a significantly better success rate at the end of the training process over the RL model trained in the same maps (RL_{123}). The R-IL models also reach the final performance of RL_{123} after less than one fifth of the iterations (≈ 200) and thus confirm our initial hypothesis that the IL initialization can significantly reduce the training time in RL applications. In CPO the exploration results from the stochasticity of the motion commands of the learned policy. Initializing RL via IL leads to significantly more efficient exploration than the one observed in plain RL. This is due to the fact that exploration through Gaussian perturbation of a nominal motion command is inherently local in the policy space. As a consequence, a better initialization will also yield informative exploratory samples in the early learning stages.

Figure 4 also shows that the final performance is affected by the initial starting state, with models initialized using more complex maps and/or more trajectories not only performing better but also learning faster. In general, it can also be seen that even a very small amount of expert demonstrations can significantly improve the overall performance.

In Figure 5, the success rate of model with typical performance according to Figure 4 ($c_{1000}+RL$) on the three individual TM training maps is evaluated. It shows how the agent quickly learns to navigate on the easy map (1) while the

success rate on the more difficult maps (2+3) remains smaller. The overall success ratio is smaller compared to Figure 4, as there multiple crashes were allowed to boost exploration. For the evaluation in Figure 5 the trajectory is aborted after each crash.

C. Simulation results

While Figures 4 and 5 show the navigation performance of the models on the training maps, the more interesting analysis comes from the investigation of how successful the learned navigation policies transfer to unseen environments. In this section, we will analyze this generalization performance in simulation. We constructed two $10\text{ m} \times 10\text{ m}$ evaluation maps as shown in Figure 6: (i) A test *maze* and (ii) an environment with thin walls and *clutter*. Both of these environments were never encountered during training.

In order to evaluate the different models, we conducted the following experiment: For each environment (*maze + clutter*), 100 random start and target positions were sampled. In order to make the results consistent, each model was evaluated given the same randomly generated positions per map. Possible outcomes for each trajectory are a *success*, a *timeout* or a *crash*. The timeout is triggered, if the target cannot be reached within 5 min — this time would allow the robot to travel 60 m with an average speed of $0.2 \frac{\text{m}}{\text{s}}$ on the $10\text{ m} \times 10\text{ m}$ map. The resulting trajectories of the evaluation with model $c_{1000}+RL$ on both maps are visualized in Figure 6.

Based on the 200 evaluation trajectories per model, Figure 7 presents the resulting statistics. Similar to the results on the training maps, the R-IL models outperform all the other models w.r.t. their success ratio. The model with 1000 expert demonstrations in the *complex* environment combined with 1000 RL iterations ($c_{1000}+RL$) shows the best generalization performance. However, Figure 7 also shows that only 10 expert demonstrations are enough to end up with a considerably better model ($s_{10}+RL$) compared to pure RL. Furthermore, as the comparison of the $R-IL_{200}$ and pure RL models suggests, if pre-training is conducted, the training time of plain RL can be reduced by at least a factor of five in our application while still providing a better navigation performance compared to standard RL training on the unseen maps. The $s_{10}+RL_{200}$ model, which only has seen 10 expert demonstrations and was

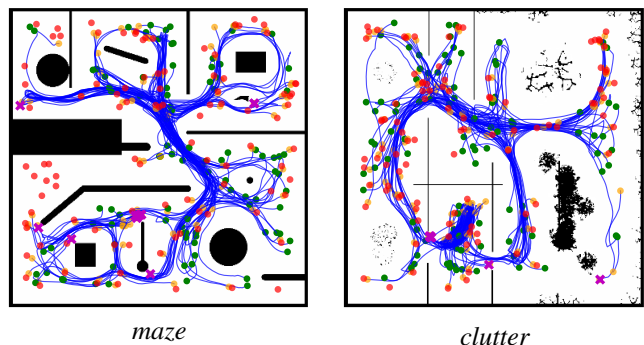


Fig. 6: Evaluation runs between 100 randomly sampled start and target positions on the two unknown test maps (both $10\text{ m} \times 10\text{ m}$). This evaluation was done with all the models, yet the one used for visualization is $c_{1000}+RL$. The trajectories are shown in blue, the starting positions in green, the set targets in red, the trajectory end points in yellow and crashes as magenta crosses.

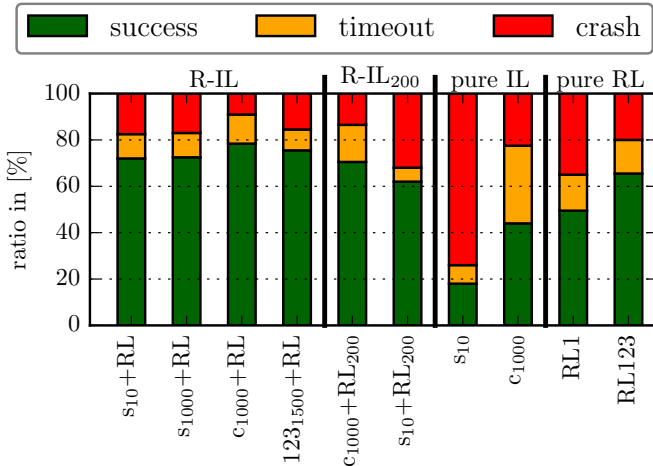


Fig. 7: Evaluation results of 200 trajectories on the previously unseen test maps (100 each) as shown in Figure 6. The outcome of each trajectory can be a success, a timeout (not reaching the target after 5 min), or a crash. The models are split in four categories: R-IL, where IL is combined with 1000 RL iterations; R-IL₂₀₀, with 200 RL iterations only, pure IL, and pure RL on different maps. More details of the models can be found in Table I.

trained for 200 RL steps, reaches about the same performance as the RL123 model on an unseen test map, which was trained for 1000 steps. The RL1 model, which reached a high success rate during training, does not generalize properly to other environments. The IL methods, that suffer from the distribution mismatch problem, do not generalize as well as RL based approaches.

Overall it can be said, that R-IL improves the navigation performance compared to its plain counterparts. Plain IL is target driven but suffers from a high crash rate. Plain RL ends up with a lower crash rate due to the collision constraint yet struggles to reach the target. R-IL combines the best of both worlds by making the exploration more efficient and ends up with a target driven but safer navigation solution. By only taking into account local measurements and a relative target, the final R-IL models end up with a success rate of at least 70% in previously unseen environments.

D. Real-world experiments

Moving to the real world scenarios further shows the generalization capabilities of the models and also their robustness against sensor noise and actuation delays. The platform used for our real-world tests was described in Section IV-A. The models are purely trained in simulation and the real-world test environment is unknown to the agents.

A quantitative analysis of the trajectories is provided in Table II, where the number of crashes, the amount of manual joystick interference and also the comparison of the learning-

TABLE II: Results from the real-world experiments, as shown in Figure 8. d_{RC} stands for the remote controlled (joystick) distance, λd_{MB} for the relative distance compared to *move_base* and λt_{MB} for the relative time compared to *move_base*

model	#crash	d_{RC} [m]	λd_{MB}	λt_{MB}
s10+RL	0	0.0	1.15	2.39
c1000+RL	1	0.0	1.37	2.09
c1000	4	0.96	1.39	1.68
RL123	4	0.0	1.41	3.47

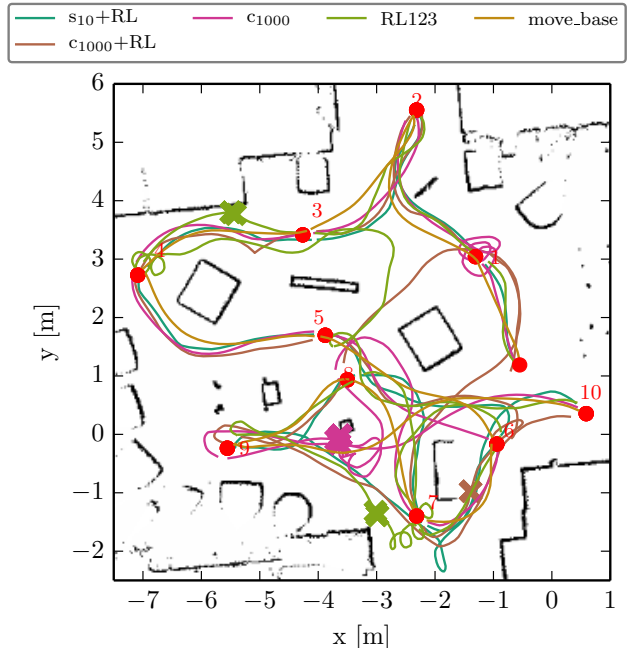


Fig. 8: Trajectories driven with the real robotic platform for a subset of the models analyzed in Figure 7. Red dots depict the numbered target positions, crosses in trajectory colors show crashes of the corresponding agents.

based trajectories compared to the ones taken by the grid-based *move_base* planning module (which uses global map information) are listed. The manual joystick interference is required since in some situations the agents get stuck and cannot be re-spawned as in simulation. If there was no motion command sent by the autonomous agent for 10 seconds, a human operator moved the robot until it was able to navigate autonomously again.

While the pure RL model tends to be more cautious — which results in a larger factor λt_{MB} — the IL model drives significantly faster but also less safely. Although the amount of crashes is the same, Figure 8 and our observations during the tests showed that the type of crashes under the IL policy are significantly worse than under the RL123 policy. While the RL123 agent only slightly brushes the walls on its side, the IL agent fully hits the obstacles. This clearly shows the benefit of using RL, which can actively constrain collisions during training and does not only resort to an implicit collision avoidance by expert imitation.

The R-IL models show a more robust and better performance than the other models, in comparison with the graph-based planner. In addition, the agent never gets stuck and no manual joystick interference was required, both with the RL123 and R-IL agents. The R-IL agents are more cautious than the expert planner, which is reflected in the longer trajectory durations (higher λt_{MB}) and results from the enforced collision constraint during training.

V. CONCLUSION

In this work, we presented a learning-based approach for map-less target driven navigation. It is based on an end-to-end model mapping from raw sensor measurements and a relative target location to motion commands of a robotic platform. In order to find this complex mapping function, we rely on neural networks which are trained using a combination of

imitation and reinforcement learning. This work shows that the combination of both can improve the sample complexity of reinforcement learning while conserving its benefits such as enforcing safety through constraints.

We show both in simulation and real-world experiments that the target-driven demonstrations through imitation learning significantly boost the exploration during reinforcement learning, resulting in either shorter training time or better overall performance given the same training time. Our results support the intuition that more expert demonstrations result in faster learning and a better navigation performance, especially in unseen environments. Yet they also show, that as few as 10 expert demonstrations can be enough to outperform pure reinforcement learning.

Plain reinforcement learning was able to show a good navigation performance on simple training maps. However, when moving towards more complex training maps and on the test maps, the pre-training through imitation learning proved to be beneficial for the exploration strategy, which improves the training times and the final navigation performance.

Our trained navigation models are able to reliably navigate in unseen environments, both in simulation and the real world. We do not recommend to replace global planning if a map is available, yet this work shows the current state of what is possible using only local information for navigation scenarios, where no environment map is available.

While in this work, training was purely conducted in simulation, in future work we will investigate how human demonstrations can be leveraged. Furthermore, we will investigate how this navigation method can be extended to dynamic environments.

REFERENCES

- [1] S. M. LaValle, *Planning algorithms*. Cambridge university press, 2006.
- [2] M. Pfeiffer, et al., "From perception to decision: A data-driven approach to end-to-end motion planning for autonomous ground robots," in *Proc. of IEEE Int. Conf. on Robotics and Automation (ICRA)*. IEEE, 2017, pp. 1527–1533.
- [3] L. Tai, et al., "Virtual-to-real deep reinforcement learning: Continuous control of mobile robots for mapless navigation," in *Intelligent Robots and Systems (IROS), 2017 IEEE/RSJ International Conference on*. IEEE, 2017, pp. 31–36.
- [4] U. Muller, et al., "Off-road obstacle avoidance through end-to-end learning," in *Advances in neural information processing systems*, 2005, pp. 739–746.
- [5] V. Mnih, et al., "Asynchronous methods for deep reinforcement learning," in *International Conference on Machine Learning*, 2016, pp. 1928–1937.
- [6] D. B. Grimes and R. P. Rao, "Learning actions through imitation and exploration: Towards humanoid robots that learn from humans," in *Creating Brain-Like Intelligence*. Springer, 2009, pp. 103–138.
- [7] J. Achiam, et al., "Constrained policy optimization," *arXiv preprint arXiv:1705.10528*, 2017.
- [8] P. Abbeel, et al., "Apprenticeship learning for motion planning with application to parking lot navigation," in *Proc. of IEEE/RSJ Int. Conf. on Intelligent Robots and Systems (IROS)*, Nice, France, Sept. 2008, pp. 1083–1090.
- [9] M. Pfeiffer, et al., "Predicting actions to act predictably: Cooperative partial motion planning with maximum entropy models," in *Proc. of IEEE/RSJ Int. Conf. on Intelligent Robots and Systems (IROS)*. IEEE, Oct. 2016, pp. 2096–2101.
- [10] H. Kretzschmar, et al., "Socially compliant mobile robot navigation via inverse reinforcement learning," *The International Journal of Robotics Research*, vol. 35, no. 11, pp. 1289–1307, 2016.
- [11] M. Wulfmeier, et al., "Watch this: Scalable cost-function learning for path planning in urban environments," in *Intelligent Robots and Systems (IROS), 2016 IEEE/RSJ International Conference on*. IEEE, 2016, pp. 2089–2095.
- [12] C. Chen, et al., "Deepdriving: Learning affordance for direct perception in autonomous driving," in *Proc. of the IEEE Int. Conf. on Computer Vision (ICCV)*, 2015, pp. 2722–2730.
- [13] D. K. Kim and T. Chen, "Deep neural network for real-time autonomous indoor navigation," *arXiv preprint arXiv:1511.04668*, 2015.
- [14] J. Sergeant, et al., "Multimodal deep autoencoders for control of a mobile robot," in *Proc. of Australasian Conf. for Robotics and Automation (ACRA)*, 2015.
- [15] S. Ross, et al., "A reduction of imitation learning and structured prediction to no-regret online learning," in *Proceedings of the fourteenth international conference on artificial intelligence and statistics*, 2011, pp. 627–635.
- [16] —, "Learning monocular reactive uav control in cluttered natural environments," in *Proc. of IEEE Int. Conf. on Robotics and Automation (ICRA), 2013*. IEEE, 2013, pp. 1765–1772.
- [17] B. Bischoff, et al., "Hierarchical reinforcement learning for robot navigation," in *ESANN*, 2013.
- [18] B. Zuo, et al., "A reinforcement learning based robotic navigation system," *2014 IEEE International Conference on Systems, Man, and Cybernetics (SMC)*, pp. 3452–3457, 2014.
- [19] P. Mirowski, et al., "Learning to navigate in complex environments," *International Conference on Learning Representations*, 2017.
- [20] J. Bruce, et al., "One-shot reinforcement learning for robot navigation with interactive replay," *CoRR*, vol. abs/1711.10137, 2017.
- [21] J. Zhang, et al., "Deep reinforcement learning with successor features for navigation across similar environments," *2017 IEEE/RSJ International Conference on Intelligent Robots and Systems (IROS)*, pp. 2371–2378, 2017.
- [22] Y. Zhu, et al., "Target-driven visual navigation in indoor scenes using deep reinforcement learning," *2017 IEEE International Conference on Robotics and Automation (ICRA)*, pp. 3357–3364, 2017.
- [23] B. Balaguer and S. Carpin, "Combining imitation and reinforcement learning to fold deformable planar objects," *2011 IEEE/RSJ International Conference on Intelligent Robots and Systems*, pp. 1405–1412, 2011.
- [24] Y. Zhu, et al., "Reinforcement and imitation learning for diverse visuomotor skills," *CoRR*, vol. abs/1802.09564, 2018.
- [25] R. J. Williams, "Simple statistical gradient-following algorithms for connectionist reinforcement learning," in *Reinforcement Learning*. Springer, 1992, pp. 5–32.
- [26] J. Schulman, et al., "Trust region policy optimization," in *International Conference on Machine Learning*, 2015, pp. 1889–1897.
- [27] E. W. Dijkstra, "A note on two problems in connexion with graphs," *Numerische mathematik*, vol. 1, no. 1, pp. 269–271, 1959.
- [28] D. Amodè, et al., "Concrete problems in ai safety," *arXiv preprint arXiv:1606.06565*, 2016.
- [29] Y. Zhu, et al., "Target-driven visual navigation in indoor scenes using deep reinforcement learning," in *Robotics and Automation (ICRA), 2017 IEEE International Conference on*. IEEE, 2017, pp. 3357–3364.
- [30] M. Quigley, et al., "Ros: an open-source robot operating system," in *ICRA workshop on open source software*. Kobe, Japan, 2009, p. 5.
- [31] R. Vaughan, "Massively multi-robot simulation in stage," *Swarm intelligence*, vol. 2, no. 2-4, pp. 189–208, 2008.